INTERNATIONAL JOURNAL FOR NUMERICAL METHODS IN FLUIDS, VOL. 15, 817–838 (1992)

DRIFT FORCES ON A PAIR OF VERTICAL CYLINDERS

M. RAHMAN

Department of Applied Mathematics, Technical University of Nova Scotia, Halifax, Nova Scotia, Canada B3J 2X4

M. G. SATISH

Department of Civil Engineering, Technical University of Nova Scotia, Halifax, Nova Scotia, Canada B3J 2X4

W. PERRIE

Physical and Chemical Sciences, Scotia-Fundy Region, Department of Fisheries and Oceans, Bedford Institute of Oceanography, Dartmouth, Nova Scotia, Canada B2Y 4A2

AND

J. ZHU

Department of Civil Engineering, Technical University of Nova Scotia, Halifax, Nova Scotia, Canada B3J 2X4

SUMMARY

An approximate method is presented here for estimating the hydrodynamic second-order drift forces on a pair of bottom-mounted, surface-piercing circular cylinders in water of arbitrary uniform depth. The theoretical results are based upon the large-spacing approximation. Results are presented to illustrate the influence of the various wave and structural parameters on the hydrodynamic forces on each of the cylinders.

KEY WORDS Diffraction Drift forces Hydrodynamic forces Offshore structures Second order

INTRODUCTION

The problem of hydrodynamic interactions within a group of large multicomponent offshore structures subjected to ocean waves has been worked on by various research groups over the last few years. From practical considerations it is extremely important to be able to predict the wave loads on multicolumn structures in waves. When many offshore structures are placed together in a configuration, the hydrodynamic loads on individual components may be significantly different from the loading they would each experience in isolation. This is simply because of the hydrodynamic coupling between the bodies.

As early as in 1977, Budal[1] studied the wave energy absorption for the three-dimensional case, considering linear arrays or rows of equidistant structures. The theoretical aspects of the more general case of wave power absorption by an array of equispaced equal groups of oscillating structures were considered by Falnes.[2] Ohkusu[3] used the method of multiple scattering in which the scattered potential is determined from each scattering event within the cylinder group. Spring and Monkmeyer[4] adopted a similar approach to evaluate the first-order wave forces on a closely spaced group of vertical cylinders. A series solution was obtained, the coefficients of which were determined from a set of matrix equations. Results were given for two cylinders in various

0271–2091/92/190817–22$16.00

Received November 1991
Revised May 1992

configurations relative to the incident wave angles. Chakrabarti[5] later used the same method for the derivation of the velocity potential for any number of cylinders in the presence of linear waves.

Simon[6] proposed an approximate theory for computing wave forces on an array of wave energy devices. According to this theory, a diverging wave scattering from one cylinder is replaced by a plane wave of appropriate amplitude in the vicinity of another cylinder. Once the amplitude and phase of the equivalent plane wave have been determined, the problem reduces to summing the effects of the plane waves on any given cylinder. The effect of this equivalent plane wave on the given cylinder is then computed. The solution inherently assumes that the spacing between two cylinders is fairly large relative to the incident wavelength. More recently, McIver and Evans[7] formulated a new matrix method based upon the idea of Simon[6] for the linear multicylinder problem. In this method the efficiency is improved by approximating the effect on one cylinder of scattered waves from other cylinders as that of plane incident waves. Their numerical solution for three cylinders gives good results even when the cylinders are close to one another.

The previous analysis for multiple scattering in arrays is restricted to the linearized (small-amplitude) wave theory only. However, the hydrodynamic interactions caused by non-linear (finite amplitude) wave theory are not well understood and to our knowledge have not been reported in the literature. Most of the previous investigations in this area have been directed towards extending the linear theory of MacCamy and Fuchs[8] for an isolated, bottom-mounted, surface-piercing cylindrical pile to include second-order terms in the analysis.[9-12] Recently, Masuda *et al.*[13, 14] have presented a numerical technique to calculate the second-order diffraction loads on arrays of vertical cylinders of arbitrary cross-sections. The method requires a numerical integration over the entire mean fluid free surface and this is computationally very expensive.

In the present paper a method is formulated to estimate the hydrodynamic forces to second order on a pair of bottom-mounted, surface-piercing cylinders in water of arbitrary uniform depth. The second-order drift forces are calculated using an extension of Lighthill's method[15] for finite water depth. The first-order potentials on each cylinder are now adjusted to take into account hydrodynamic interference effects. In Lighthill's technique the explicit calculation of the second-order potential is not required. Theoretical results are presented which illustrate the influence of the relative spacing between the cylinders, the radius of the cylinders and the incident wave frequency on the hydrodynamic loads to second order.

MATHEMATICAL FORMULATION

In this paper we consider two right circular cylinders of radius a separated by a distance s. We assume that these cylinders extend from the ocean bed to the free surface as shown in Figure 1. A fixed co-ordinate system $0xyz$ is employed with the x- and y-axes in the horizontal plane and the z-axis pointing vertically upwards from an origin on the free surface. The centres of the two cylinders, O_1 and O_2, lie on Oy. The water depth is h. Long-crested sinusoidal waves of frequency σ and amplitude A propagate in the positive x-direction.

The linear velocity potential Φ may be written

$$\Phi = \mathrm{Re}(\phi e^{i\sigma t}), \tag{1}$$

where Re stands for the real part of ( ). The fluid velocities $\boldsymbol{q} = \nabla\Phi$. The potential ϕ is conveniently decomposed into contributions ϕ_I and ϕ_S from incident and scattered waves respectively. In terms of cylindrical co-ordinates r_1, θ_1, and z we may express ϕ_I relative to the centre of cylinder 1 as

$$\phi_I(r_1, \theta_1, z) = \frac{gA}{\sigma} \frac{\cosh[k(z+h)]}{\cosh(kh)} \sum_{n=-\infty}^{\infty} (-i)^n J_n(kr_1)\exp(in\theta_1), \tag{2}$$

where J_n is a Bessel function of the first kind.

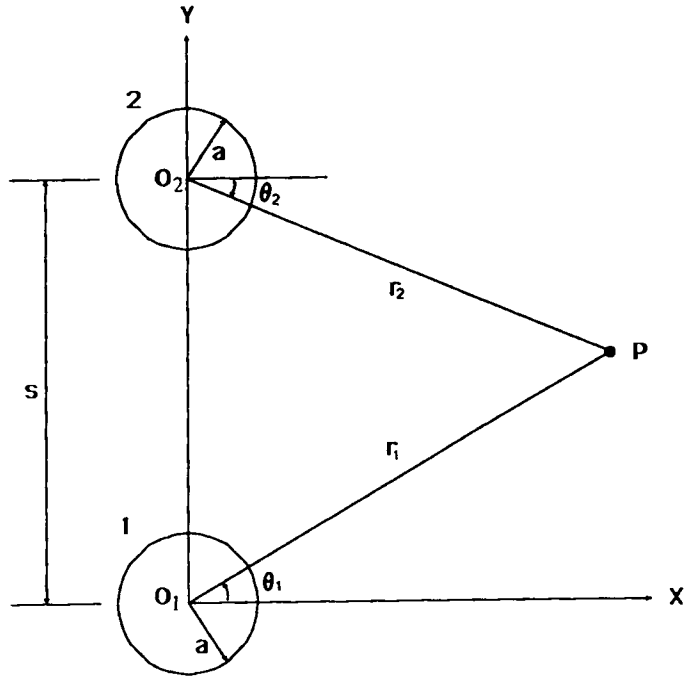

Figure 1. Co-ordinate systems for two cylinders

The far-field scattered potential due to cylinder 1 may be written

$$\phi_{S1}(r_1,\theta_1,z)=\frac{gA}{\sigma}\frac{\cosh[k(z+h)]}{\cosh(kh)}\sum_{n=-\infty}^{\infty}a_n(-\mathrm{i})^n H_n^{(2)}(kr_1)\exp(\mathrm{i}n\theta_1). \tag{3}$$

Here $\sigma^2/g=k\tanh(kh)$ is the dispersion relation and k is the wave number, $H_n^{(2)}$ is a Hankel function of the second kind satisfying the radiation condition, and the coefficients a_n are to be determined from the boundary condition on the cylinder.

In view of the symmetry about $0x$, the scattered potential due to cylinder 2 must be expressible in terms of cylindrical co-ordinates r_2, θ_2 and z in the same form as (3):

$$\phi_{S2}(r_2,\theta_2,z)=\frac{gA}{\sigma}\frac{\cosh[k(z+h)]}{\cosh(kh)}\sum_{n=-\infty}^{\infty}a_n(-\mathrm{i})^n H_n^{(2)}(kr_2)\exp(\mathrm{i}n\theta_2). \tag{4}$$

Equation (4) can be conveniently transformed into co-ordinates r_1, θ_1 and z using the Graf addition theorem for Bessel functions (equation 9.1.79 given by Abramowitz and Stegun[16]). Referring to the geometry of Figure 1, we can write

$$H_n^{(2)}(kr_2)\exp\left[-\mathrm{i}n\left(\frac{\pi}{2}-\theta_2\right)\right]=\sum_{m=-\infty}^{\infty}H_{m+n}^{(2)}(ks)J_m(kr_1)\exp\left[-\mathrm{i}m\left(\frac{\pi}{2}-\theta_1\right)\right]. \tag{5}$$

Thus equation (4) is transferred into

$$\phi_{S2}(r_1,\theta_1,z)=\frac{gA}{\sigma}\frac{\cosh[k(z+hz)]}{\cosh(kh)}\sum_{n=-\infty}^{\infty}a_n\sum_{m=-\infty}^{\infty}(-\mathrm{i})^m H_{m+n}^{(2)}(ks)J_m(kr_1)\exp(\mathrm{i}m\theta_1). \tag{6}$$

This then can be treated as the second scattered potential due to cylinder 1 such that the total potential is $\phi=\phi_I+\phi_{S1}+\phi_{S2}$.

The body surface boundary condition at cylinder 1 is

$$\frac{\partial\phi}{\partial r_1}=0, \quad \text{i.e.} \ \frac{\partial}{\partial r_1}(\phi_I+\phi_{S1}+\phi_{S2})=0 \quad \text{at } r_1=a. \tag{7}$$

Substitution of (2), (3) and (6) into (7) yields

$$\sum_{n=-\infty}^{\infty}(-\mathrm{i})^n J_n'(ka)\exp(\mathrm{i}n\theta_1)+\sum_{n=-\infty}^{\infty}a_n(-\mathrm{i})^n H_n^{(2)\prime}(ka)\exp(\mathrm{i}n\theta_1),$$

$$+\sum_{n=-\infty}^{\infty}a_n\sum_{m=-\infty}^{\infty}(-\mathrm{i})^m H_{m+n}^{(2)}(ks)J_m'(ka)\exp(\mathrm{i}m\theta_1)=0, \tag{8}$$

which holds for all θ_1 in the range $(0, 2\pi)$. Rearranging this equation and interchanging the order of the two convergent summations, we obtain equations for a_n:

$$a_n\frac{H_n^{(2)\prime}(ka)}{J_n'(ka)}+\sum_{m=-\infty}^{\infty}a_m H_{m+n}^{(2)}(ks)=-1, \quad -\infty<n<\infty, \tag{9}$$

where n is an integer. Therefore the combined velocity potential $\phi=\phi_I+\phi_{S1}+\phi_{S2}$ expressed in co-ordinates r_1, θ_1 and z is then given by

$$\phi(r_1,\theta_1,z)=\frac{gA}{\sigma}\frac{\cosh[k(z+h)]}{\cosh(kh)}\sum_{n=-\infty}^{\infty}(-\mathrm{i})^n\exp(\mathrm{i}n\theta_1)$$

$$\times\left(J_n(kr_1)+a_n H_n^{(2)}(kr_1)+\sum_{m=-\infty}^{\infty}a_m H_{m+n}^{(2)}(ks)J_n(kr_1)\right). \tag{10}$$

This corresponds to the incident wave plus the total effect of scattering by the two cylinders. With the aid of (9) this may be written in the simple form

$$\phi(r_1,\theta_1,z)=\frac{gA}{\sigma}\frac{\cosh[k(z+h)]}{\cosh(kh)}\sum_{n=-\infty}^{\infty}a_n\left(H_n^{(2)}(kr_1)-\frac{H_n^{(2)\prime}(ka)}{J_n'(ka)}J_n(kr_1)\right)\exp\left[\mathrm{i}\left(n\theta_1-n\frac{\pi}{2}\right)\right]. \tag{11}$$

On the surface of cylinder 1 the expression for $\phi(a, \theta, z)$ then becomes

$$\phi(a,\theta,z)=\frac{gA}{\sigma}\frac{\cosh[k(z+h)]}{\cosh(kh)}\sum_{n=-\infty}^{\infty}\frac{a_n}{J_n'(ka)}\exp\left[\mathrm{i}\left(n\theta_1-\frac{n}{2}\pi\right)\right]\frac{2\mathrm{i}}{\pi ka}. \tag{12}$$

Equations (11) and (12) are the complex form of the linear velocity potential. The real form of this potential with the frequency σ is given by

$$\Phi(r_1,\theta_1,z,t)=\frac{gA}{\sigma}\frac{\cosh[k(z+h)]}{\cosh(kh)}\mathrm{Re}\left\{\sum_{n=-\infty}^{\infty}a_n\left(H_n^{(2)}(kr_1)-\frac{H_n^{(2)\prime}(ka)}{J_n'(ka)}J_n(kr_1)\right)\right.$$

$$\left.\times\exp\left[\mathrm{i}\left(n\theta_1+\sigma t-\frac{n\pi}{2}\right)\right]\right\}. \tag{13}$$

In the following we shall find the first-order forces. Using Lighthill's technique,[15] the second-order drift forces will be obtained from the knowledge of the linear potential Φ alone. The difficulty in determining these forces lies in the evaluation of the coefficients a_n.

FIRST-ORDER WAVE FORCES

The first-order forces on cylinder 1 can be determined from the linearized Bernoulli equation as

$$F_x^{(1)} = \int_{-h}^{0} \int_{0}^{2\pi} \left(-\rho \frac{\partial \Phi}{\partial t} \right) (a \cos\theta) \mathrm{d}\theta \, \mathrm{d}z, \tag{14}$$

$$F_y^{(1)} = \int_{-h}^{0} \int_{0}^{2\pi} \left(-\rho \frac{\partial \Phi}{\partial t} \right) (a \sin\theta) \mathrm{d}\theta \, \mathrm{d}z, \tag{15}$$

where $F_x^{(1)}$ and $F_y^{(1)}$ denote the components of horizontal force along the x and y-directions respectively.

By substituting (13) into (14) and (15), we readily derive the exact first-order linear forces as

$$F_x^{(1)} = -\frac{2\rho g A}{k^2 J_1'(ka)} \tanh(kh) \mathrm{Re}[(a_1 + a_{-1}) \mathrm{e}^{\mathrm{i}(\sigma t + \pi/2)}], \tag{16}$$

$$F_y^{(1)} = \frac{2\rho g A}{k^2 J_1'(ka)} \tanh(kh) \mathrm{Re}[(a_1 - a_{-1}) \mathrm{e}^{\mathrm{i}\sigma t}]. \tag{17}$$

For an isolated cylinder equation (9) reduces to

$$a_n \frac{H_n^{(2)\prime}(ka)}{J_n'(ka)} = -1, \tag{18}$$

from which it is clear that

$$a_n = a_{-n} \tag{19}$$

and hence

$$a_1 = a_{-1}. \tag{20}$$

Therefore we obtain

$$F_y^{(1)} = 0, \qquad F_x^{(1)} = C_M(\rho g A \pi a^2) \tanh(kh) \cos(\sigma t - \beta), \tag{21}$$

where

$$C_M = \frac{4}{\pi k^2 a^2 \sqrt{[J_1'^2(ka) + Y_1'^2(ka)]}}, \tag{22}$$

$$\beta = \tan^{-1}\left(\frac{J_1'}{Y_1'} \right). \tag{23}$$

These results are the same as the previously published results.[8]

We can therefore define the amplification factors due to first-order forces for two cylinders compared to the first-order force $|F|$ for a single cylinder as

$$\lambda_x = |F_x^{(1)}|/|f|, \tag{24}$$

$$\lambda_y = |F_y^{(1)}|/|f|, \tag{25}$$

where $|f| = |C_M(\rho g A \pi a^2) \tanh(kh) \cos(\sigma t - \beta)|$. These are evaluated numerically in Table I.

SECOND-ORDER WAVE FORCES

Referring to the work of Lighthill,[15] we can determine the second-order drift forces by considering (a) the waterline force and (b) the dynamic force. We shall discuss these forces separately.

Table I. Numerical results of amplification factors for various parameters; $s/a=5$, $h/a=3$

ka	ks	kh	μ_x	μ_y	λ_x	λ_y
0·50	2·50	1·50	1·296572	0·020009	0·965637	0·110587
0·60	3·00	1·80	1·039462	−0·098980	0·939990	0·129585
0·70	3·50	2·10	0·870259	−0·1235236	0·933213	0·136623
0·80	4·00	2·40	0·783540	−0·106307	0·945425	0·141666
0·90	4·50	2·70	0·752349	−0·065245	0·970223	0·150065
1·00	5·00	3·00	0·755871	−0·001490	0·997097	0·163120
1·10	5·50	3·30	0·781834	0·078732	1·016313	0·180453
1·20	6·00	3·60	0·833345	0·157476	1·023968	0·200459
1·30	6·50	3·90	0·924884	0·208889	1·022195	0·220331
1·40	7·00	4·20	1·053781	0·210658	1·015537	0·237171
1·50	7·50	4·50	1·181923	0·158663	1·008307	0·250156
1·60	8·00	4·80	1·264259	0·067411	1·004103	0·261446
1·70	8·50	5·10	1·282858	−0·047339	1·005507	0·274717
1·80	9·00	5·40	1·241272	−0·180359	1·012547	0·293005
1·90	9·50	5·70	1·143017	−0·327039	1·021617	0·316342
2·00	10·00	6·00	0·995994	−0·452463	1·027404	0·337502

These two forces can easily be obtained from the knowledge of the first-order linear potential given by Bernoulli's equation. The corresponding free surface elevation is given by

$$\eta(r_1,\theta_1,t)=\mathrm{Re}\left\{A\sum_{n=-\infty}^{\infty}a_n\left(H_n^{(2)}(kr_1)-\frac{H_n^{(2)\prime}(ka)}{J_n'(ka)}J(kr_1)\right)\exp\left[\mathrm{i}\left(n\theta_1+\sigma t-(n+1)\frac{\pi}{2}\right)\right]\right\}. \tag{26}$$

The horizontal components of the waterline forces can be determined from the formulae

$$F_{wx}^{(2)}=\int_0^{2\pi}\frac{\rho}{2g}\left(\frac{\partial\Phi}{\partial t}\right)^2_{\substack{r_1=a\\z=0}}(-a\cos\theta)\mathrm{d}\theta=-\frac{\rho gA^2}{a\pi^2k^2}\mathrm{Re}\left(\int_0^{2\pi}(\phi^2\mathrm{e}^{2\mathrm{i}\sigma t}+\phi\phi^*)\cos\theta\,\mathrm{d}\theta\right), \tag{27}$$

$$F_{wy}^{(2)}=\int_0^{2\pi}\frac{\rho}{2g}\left(\frac{\partial\Phi}{\partial t}\right)^2_{\substack{r_1=a\\z=0}}(-a\sin\theta)\mathrm{d}\theta=-\frac{\rho gA^2}{a\pi^2k^2}\mathrm{Re}\left(\int_0^{2\pi}(\phi^2\mathrm{e}^{2\mathrm{i}\sigma t}+\phi\phi^*)\sin\theta\,\mathrm{d}\theta\right). \tag{28}$$

At $z=0$ and $r_1=a$ the expression for ϕ is

$$\phi=\frac{2gA}{\pi ka\sigma}\sum_{n=-\infty}^{\infty}\frac{a_n}{J_n'(ka)}\exp\left[-\mathrm{i}\left(n\theta-(n-1)\frac{\pi}{2}\right)\right]. \tag{29}$$

It is to be noted here that $\Phi=\mathrm{Re}(\phi\mathrm{e}^{\mathrm{i}\sigma t})$, where Φ is a real function, ϕ is a complex function and ϕ^* is its complex conjugate.

By substituting equation (29) and performing integration with respect to θ in (27) and (28), we may write these in the form

$$F_{wx}^{(2)}=-\frac{\rho gA^2}{\pi ak^2}\mathrm{Re}\left[\mathrm{i}\mathrm{e}^{2\mathrm{i}\sigma t}\sum_{n=-\infty}^{\infty}\frac{a_n}{J_n'}\left(\frac{a_{-1-n}}{J'_{-1-n}}-\frac{a_{1-n}}{J'_{1-n}}\right)+\mathrm{i}\sum_{n=-\infty}^{\infty}\frac{a_n}{J_n'}\left(\frac{a_{n+1}^*}{J'_{n+1}}-\frac{a_{n-1}^*}{J'_{n-1}}\right)\right], \tag{30}$$

$$F_{wy}^{(2)}=-\frac{\rho gA^2}{\pi ak^2}\mathrm{Re}\left[\mathrm{e}^{2\mathrm{i}\sigma t}\sum_{n=-\infty}^{\infty}\frac{a_n}{J_n'}\left(\frac{a_{-1-n}}{J'_{-1-n}}+\frac{a_{1-n}}{J'_{1-n}}\right)+\sum_{n=-\infty}^{\infty}\frac{a_n}{J_n'}\left(\frac{a_{n+1}^*}{J'_{n+1}}+\frac{a_{n-1}^*}{J'_{n-1}}\right)\right]. \tag{31}$$

Similarly, the horizontal components of the dynamic forces may be obtained from the formulae

$$F_{dx}^{(2)} = \int_0^{2\pi} \left(\int_{-h}^{0} \frac{-\rho}{2} (\nabla\Phi)^2 \, dz \right) (-a\cos\theta) \, d\theta, \tag{32}$$

$$F_{dy}^{(2)} = \int_0^{2\pi} \left(\int_{-h}^{0} \frac{-\rho}{2} (\nabla\Phi)^2 \, dz \right) (-a\sin\theta) \, d\theta. \tag{33}$$

Performing the indicated integrations in (32) and (33), we may write these as

$$\begin{aligned} F_{dx}^{(2)} = \frac{\rho g A^2}{2\pi a k^2} \Bigg[& \mathrm{Re}\Bigg\{ \Bigg[\sum_{n=-\infty}^{\infty} \left(1 - \frac{2kh}{\sinh(2kh)}\right) \frac{a_n}{J_n'} \left(\frac{a_{1-n}}{J_{1-n}'} - \frac{a_{-1-n}}{J_{-1-n}'} \right) \\ & + \left(1 + \frac{2kh}{\sinh(2kh)}\right) \frac{a_n}{J_n'} \left(\frac{n(n-1)}{k^2a^2} \frac{a_{1-n}}{J_{1-n}'} - \frac{n(n+1)}{k^2a^2} \frac{a_{-1-n}}{J_{-1-n}'} \right) \Bigg] i e^{2i\sigma t} \Bigg\} \\ & + \mathrm{Re}\Bigg[i \sum_{n=-\infty}^{\infty} \left(1 - \frac{2kh}{\sinh(2kh)}\right) \frac{a_n}{J_n'} \left(-\frac{a_{n-1}^*}{J_{n-1}'} + \frac{a_{n+1}^*}{J_{n+1}'} \right) \\ & + \left(1 + \frac{2kh}{\sinh(2kh)}\right) \frac{a_n}{J_n'} \left(\frac{n(n+1)}{k^2a^2} \frac{a_{n+1}^*}{J_{n+1}'} - \frac{n(n-1)}{k^2a^2} \frac{a_{n-1}^*}{J_{n-1}'} \right) \Bigg] \Bigg], \end{aligned} \tag{34}$$

$$\begin{aligned} F_{dy}^{(2)} = -\frac{\rho g A^2}{2\pi a k^2} \Bigg[& \mathrm{Re}\Bigg\{ \Bigg[\sum_{n=-\infty}^{\infty} \left(1 - \frac{2kh}{\sinh(2kh)}\right) \frac{a_n}{J_n'} \left(\frac{a_{1-n}}{J_{1-n}'} - \frac{a_{-1-n}}{J_{-1-n}'} \right) \\ & + \left(1 + \frac{2kh}{\sinh(2kh)}\right) \frac{a_n}{J_n'} \left(\frac{n(n+1)}{k^2a^2} \frac{a_{-1-n}}{J_{1-n}'} + \frac{n(n-1)}{k^2a^2} \frac{a_{1-n}}{J_{1-n}'} \right) \Bigg] e^{2i\sigma t} \Bigg\} \\ & - \mathrm{Re}\Bigg[\sum_{n=-\infty}^{\infty} \left(1 - \frac{2kh}{\sinh(2kh)}\right) \frac{a_n}{J_n'} \left(\frac{a_{n-1}^*}{J_{n-1}'} + \frac{a_{n+1}^*}{J_{n+1}'} \right) \\ & + \left(1 + \frac{2kh}{\sinh(2kh)}\right) \frac{a_n}{J_n'} \left(\frac{n(n-1)}{k^2a^2} \frac{a_{n-1}^*}{J_{n-1}'} + \frac{n(n+1)}{k^2a^2} \frac{a_{n+1}^*}{J_{n+1}'} \right) \Bigg] \Bigg]. \end{aligned} \tag{35}$$

Equations (30), (31), (34) and (35) contain the oscillatory and steady state parts of the solution. Eatock-Taylor and Hung[17] obtained the steady state part of the solution in the form of wave drift enhancement effects in multicolumn structures.

FORCES ON AN ISOLATED CYLINDER

For a diffracted wave the total horizontal force F_1 can be obtained from

$$F_1 = \int_{\theta=0}^{2\pi} \left(\int_{z=-h}^{0} -\rho \frac{\partial \phi_1}{\partial t} \, dz \right)_{r=a} (-\cos\theta) a \, d\theta, \tag{36}$$

where ϕ_1 is specified in Reference 11. This function is the sum of linear incident and scattered potentials for one cylinder in waves. This expression has been obtained by many researchers, including MacCamy and Fuchs.[8]

The second-order contributions may be computed by estimating F_d and F_ω. The dynamic force F_d is given as

$$F_d = \int_{\theta=0}^{2\pi} \left(\int_{z=-h}^{0} -\frac{\rho}{2} (\nabla\phi_1)^2 \, dz \right) (-\cos\theta) a \, d\theta. \tag{37}$$

Invoking the expression for ϕ_1 and carrying out z-integration of the expression $(\nabla\phi_1)^2$, we obtain[11]

$$-\frac{A^2g}{8}\sum_{m=0}^{\infty}\sum_{n=0}^{\infty}\delta_m\delta_n R_m R_n\frac{mn}{k^2a^2}\left(1+\frac{2kh}{\sinh(2kh)}\right)\cos\left((m+n)\frac{\pi}{2}+\beta_m+\beta_n-2\sigma t\right)$$
$$+\cos\left((m-n)\frac{\pi}{2}+\beta_m-\beta_n\right)[\cos(m+n)\theta-\cos(m-n)\theta]$$
$$+\frac{A^2g}{8}\sum_{m=0}^{\infty}\sum_{n=0}^{\infty}\delta_m\delta_n R_m R_n\left(1-\frac{2kh}{\sinh(2kh)}\right)\left[\cos\left((m+n)\frac{\pi}{2}+\beta_m+\beta_n-2\sigma t\right)\right.$$
$$\left.+\cos\left((m-n)\frac{\pi}{2}+\beta_m-\beta_n\right)\right][\cos(m+n)\theta+\cos(m-n)\theta], \tag{38}$$

where the Wronskian property of Bessel functions gives

$$A_m(ka)=\frac{-2\mathrm{i}}{(\pi ka)H_m^{(2)\prime}(ka)}=R_m\mathrm{e}^{-\mathrm{i}\beta_m}, \tag{39}$$

in which

$$R_m=\frac{2}{\pi ka}[J_m'^2(ka)+Y_m'^2(ka)]^{-1/2}, \tag{40}$$

$$\beta_m=\tan^{-1}\left(\frac{J_m'(ka)}{Y_m'(ka)}\right). \tag{41}$$

In view of the subsequent θ-integration described in equation (37), we require only the coefficient of $\cos\theta$ in the double summation in (38), yielding

$$\frac{4A^2g}{\pi^2k^2a^2}\sum_{l=0}^{\infty}\left[\left(1-\frac{2kh}{\sinh(2kh)}\right)+\frac{l(l+1)}{k^2a^2}\left(1+\frac{2kh}{\sinh(2kh)}\right)\right]\{E_l-(-1)^l[C_l\cos(2\sigma t)-S_l\sin(2\sigma t)]\}, \tag{42}$$

where

$$E_l=(J_l'Y_{l+1}'-J_{l+1}'Y_l')/T_l, \tag{43}$$
$$C_l=(Y_l'J_{l+1}'-Y_{l+1}'J_l')/T_l, \tag{44}$$
$$S_l=(Y_l'Y_{l+1}'-J_l'J_{l+1}')/T_l, \tag{45}$$
$$T_l=(J_l'^2+Y_l'^2)(J_{l+1}'^2+Y_{l+1}'^2) \tag{46}$$

and the Bessel function arguments are ka. Integrating with respect to θ, the total dynamic force F_d may be expressed as

$$F_d=\frac{2\rho gA^2}{\pi ak^2}\sum_{l=0}^{\infty}\left[\left(1-\frac{2kh}{\sinh(2kh)}\right)+\frac{l(l+1)}{k^2a^2}\left(1+\frac{2kh}{\sinh(2kh)}\right)\right]$$
$$\times\{E_l-(-1)^l[C_l\cos(2\sigma t)-S_l\sin(2\sigma t)]\}. \tag{47}$$

The result (47) is the sum of the steady state and oscillatory parts, which can be written as

$$F_d^{ss}=\frac{2\rho gA^2}{\pi ak^2}\sum_{l=0}^{\infty}\left[\left(1-\frac{2kh}{\sinh(2kh)}\right)+\frac{l(l+1)}{k^2a^2}\left(1+\frac{2kh}{\sinh(2kh)}\right)\right]E_l, \tag{48}$$

$$F_{\mathrm{d}}^{\mathrm{os}} = -\frac{2\rho g A^2}{\pi a k^2} \sum_{l=0}^{\infty} (-1)^l \left[\left(1 - \frac{2kh}{\sinh(2kh)} \right) + \frac{l(l+1)}{k^2 a^2} \left(1 + \frac{2kh}{\sinh(2kh)} \right) \right]$$
$$\times [C_l \cos(2\sigma t) - S_l \sin(2\sigma t)], \tag{49}$$

such that

$$F_{\mathrm{d}} = F_{\mathrm{d}}^{\mathrm{ss}} + F_{\mathrm{d}}^{\mathrm{os}}. \tag{50}$$

The waterline force F_ω may be calculated from

$$F_\omega = \int_0^{2\pi} \frac{\rho}{2g} \left(\frac{\partial \phi_l}{\partial t} \right)_{\substack{z=0 \\ r=a}}^2 (-\cos\theta) a \, \mathrm{d}\theta. \tag{51}$$

Inserting the expression for ϕ_l into (51), the term in

$$\left(\frac{\partial \phi_l}{\partial t} \right)_{\substack{z=0 \\ r=a}}^2$$

may be written as

$$-\frac{A^2 g^2}{4} \sum_{m=0}^{\infty} \sum_{n=0}^{\infty} \delta_m \delta_n R_m R_n \left[\cos\left((m+n)\frac{\pi}{2} + \beta_m + \beta_n - 2\sigma t \right) - \cos\left((m-n)\frac{\pi}{2} + \beta_m - \beta_n \right) \right]$$
$$[\cos(m+n)\theta + \cos(m-n)\theta]. \tag{52}$$

In view of the subsequent θ-integration given in (51), we require only the coefficient of $\cos\theta$ in the double summation in (52), yielding

$$\frac{8A^2 g^2}{\pi^2 k^2 a^2} \sum_{l=0}^{\infty} \{ E_l + (-1)^l [C_l \cos(2\sigma t) - S_l \sin(2\sigma t)] \}, \tag{53}$$

where E_l, C_l and S_l are as previously defined.

Integrating with respect to θ, the total waterline force F_{w} may be obtained as

$$F_{\mathrm{w}} = -\frac{4\rho g A^2}{\pi a k^2} \sum_{l=0}^{\infty} \{ E_l + (-1)^l [C_l \cos(2\sigma t) - S_l \sin(2\sigma t)] \}. \tag{54}$$

This result may be expressed as the steady state and oscillatory parts as

$$F_{\mathrm{w}} = F_{\mathrm{w}}^{\mathrm{ss}} + F_{\mathrm{w}}^{\mathrm{os}}, \tag{55}$$

where

$$F_{\mathrm{w}}^{\mathrm{ss}} = -\frac{4\rho g A^2}{\pi a k^2} \sum_{l=0}^{\infty} E_l, \tag{56}$$

$$F_{\mathrm{w}}^{\mathrm{os}} = -\frac{4\rho g A^2}{\pi a k^2} \sum_{l=0}^{\infty} (-1)^l [C_l \cos(2\sigma t - S_l \sin(2\sigma t)]. \tag{57}$$

Combining the steady state and oscillatory parts of F_{d} and F_{w}, we obtain

$$F_{\mathrm{dw}}^{\mathrm{ss}} = -\frac{2\rho g A^2}{\pi a k^2} \sum_{l=0}^{\infty} \left[\left(1 - \frac{l(l+1)}{k^2 a^2} \right) \left(1 + \frac{2kh}{\sinh(2kh)} \right) E_l \right], \tag{58}$$

$$F_{\mathrm{dw}}^{\mathrm{os}} = -\frac{2\rho g A^2}{\pi a k^2} \sum_{l=0}^{\infty} (-1)^l \left[\left(3 - \frac{2kh}{\sinh(2kh)} \right) + \frac{l(l+1)}{k^2 a^2} \left(1 + \frac{2kh}{\sinh(2kh)} \right) \right]$$
$$\times [C_l \cos(2\sigma t) - S_l \sin(2\sigma t)]. \tag{59}$$

The drift forces for a single cylinder can then be obtained as

$$F = F_{\mathrm{w}}^{\mathrm{ss}} + F_{\mathrm{d}}^{\mathrm{ss}}. \tag{60}$$

We know that the drift forces for a pair of cylinders are

$$F_x = (F_{\mathrm{wx}}^{(2)})_{\mathrm{ss}} + (F_{\mathrm{dx}}^{(2)})_{\mathrm{ss}}, \tag{61}$$

$$F_y = (F_{\mathrm{wy}}^{(2)})_{\mathrm{ss}} + (F_{\mathrm{dy}}^{(2)})_{\mathrm{ss}}. \tag{62}$$

Therefore the amplification factor for two cylinders as compared to a single cylinder can be estimated by using the definitions

$$\mu_x = F_x/F, \tag{63}$$

$$\mu_y = F_y/F. \tag{64}$$

These are computed in Table 1 and compared with λ_x and λ_y for a variety of parameter values. We also redefine the following dimensionless second-order *waterline* and *dynamic* force components respectively:

$$F_{\mathrm{wx}} = F_{\mathrm{wx}}^{(2)}/2\rho g A a^2, \tag{65}$$

$$F_{\mathrm{wy}} = F_{\mathrm{wy}}^{(2)}/2\rho g A a^2; \tag{66}$$

$$F_{\mathrm{dx}} = F_{\mathrm{dx}}^{(2)}/2\rho g A a^2, \tag{67}$$

$$F_{\mathrm{dy}} = F_{\mathrm{dy}}^{(2)}/2\rho g A a^2. \tag{68}$$

NUMERICAL RESULTS

In Figures 2(a) and 2(b) we present the variation in amplification factors defined in equations (63) and (64) as a function of ks for the pair of cylinders shown in Figure 1. We have used $s/a = 10$ in order to validate our results with the approximate calculations of Eatock-Taylor and Hung.[17] Our results are qualitatively similar to those of Eatock-Taylor and Hung. Our μ_x slightly lags the estimates they made for μ_x and our μ_y has about the same phase as their μ_y. For $ks < 1$ we obtain a larger μ_y than they compute.

The sensitivity of μ_x and μ_y to s/a as a function of ks for $kh = 30$ is shown in Figures 3(a) and 3(b). Clearly μ_x and μ_y are seen to retain the characteristic oscillatory variation shown in Figures 2(a) and 2(b). The phases of μ_x and μ_y as well as the asymptotically singular behaviour of μ_y for small ks are found to be independent of s/a for the parameters considered. As s/a increases, the amplitude of the oscillatory variation of μ_x and μ_y decreases with respect to ks compared to their behaviour when s/a is small.

Figures 4(a)–4(c) show the variation in μ_x and μ_y with respect to ka for $ks = 3$, 10 and 50 respectively when $kh = 30$ and $A/a = 2$. It is interesting that when $ks = 3$, μ_x and μ_y achieve extrema at $ka = 1{\cdot}50$, which corresponds to the two cylinders touching. Whereas μ_x varies from a value of about 1·0 to a maximum of about 1·5, μ_y is almost zero for small ka and monotonically decreases to a minimum of about $-1{\cdot}75$. Figure 4(b) shows that these are extrema of the variations in μ_x and μ_y with respect to ka when $ks = 10$. In this case μ_x is very close to 1·0 for the whole domain of ka, with only a slight maximum at about $ka = 2{\cdot}0$. Except for a minimum of about $-0{\cdot}6$, μ_y is almost 0·0 for all ka. Finally, when $ks = 50$, we present the variation is μ_x and μ_y with respect to ka in Figure 4(c). It is evident that μ_x is almost unity for all values of ka, with only a slight maximum

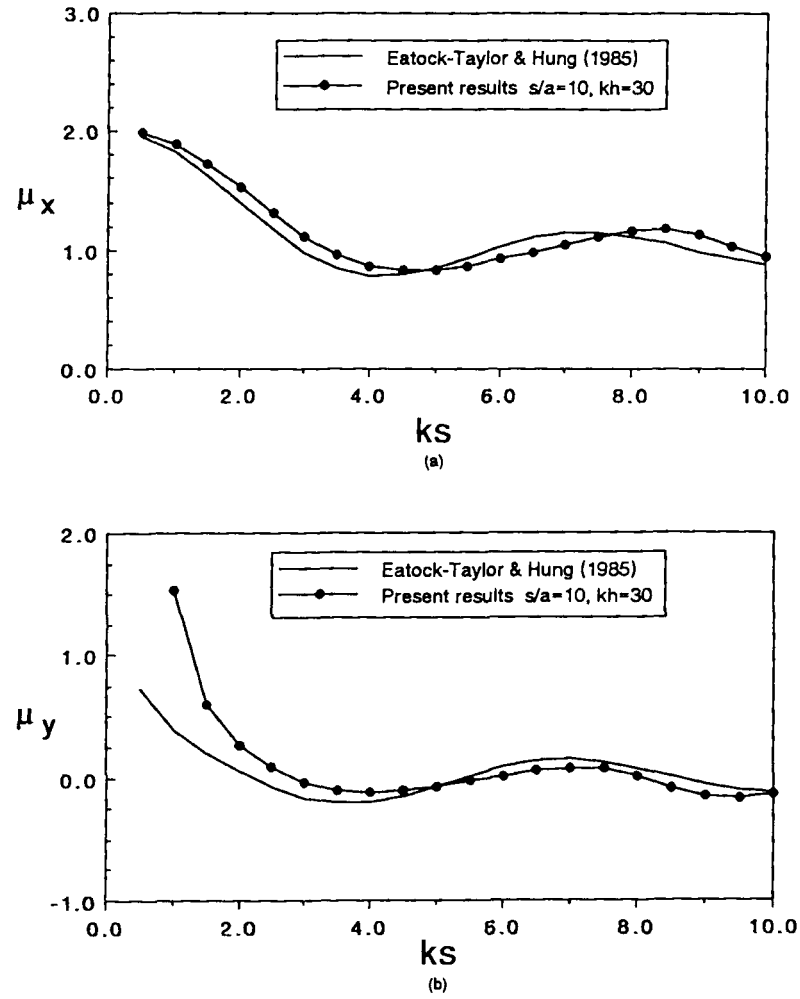

Figure 2. Comparison of amplification factors between the present results and those of Eatock-Taylor and Hung:[17] (a) μ_x, (b) μ_y

at about $ka = 7{\cdot}0$. Similarly, μ_y is almost zero for all values of ka, except for a slight minimum or series of local minima at about $ka = 12{\cdot}0$.

When ks is small, as in Figure 4(a), the extrema are most evident, whereas as ks increases, the extrema become less evident and occur at larger values of ka. Thus the ratio s/a is approximately conserved for the occurrence of these resonances. When ks is quite large, the cylinders are essentially isolated, with the result that μ_x is almost unity for all ka and μ_y is almost zero as shown in Figure 4(c). The terms "small' and 'large' ks in this context are understood in terms of separation distance relative to the incident wavelength.

In Figures 5(a), 5(b) and 6(a), 6(b) we present the absolute maximum waterline forces in the x-direction, F_{wxm}, and in the y-direction, F_{wym}, as compared to the corresponding components of the absolute maximum dynamic forces F_{dxm} and F_{dym}. These are given in equations (30), (31), (34) and (35) respectively. Interestingly, F_{wxm} is about four times F_{dxm} in magnitude and both are

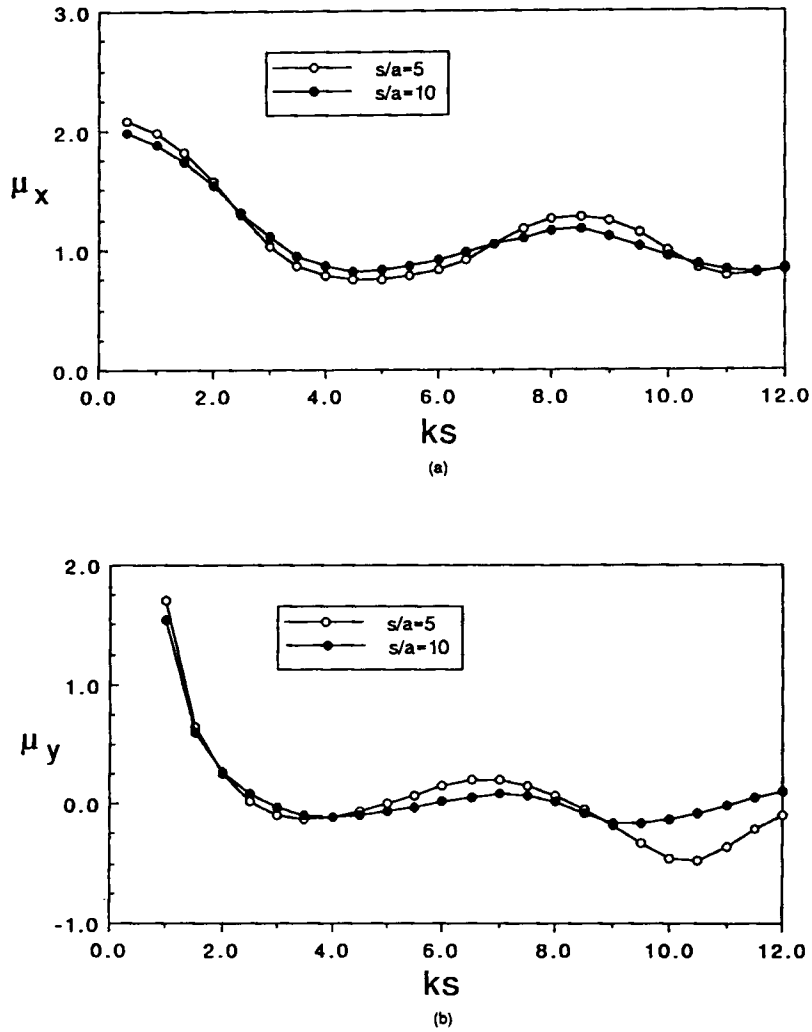

Figure 3. Amplification factors as a function of ks for $kh=30$: (a) μ_x, (b) μ_y

relatively large for small ks. While F_{wym} is several times F_{dym} in magnitude, both are quite small compared to the corresponding x-components. Both F_{wym} and F_{dym} exhibit singular behaviour as ks approaches zero, and F_{dym} seems to be much larger than F_{wym}.

The variations in F_{dxm} and F_{wxm} with ka for $kh=30$ and $A/a=2$ are shown in Figures 7(a)–7(c). Not only are both components qualitatively similar in their variation with respect to ka, they are also similar in magnitude. When $ks=3$, both components appear to achieve their maxima at $ka=1{\cdot}5$, which corresponds to the situation where the cylinders just touch. Letting $ks=10$ in Figure 7(b) shows that these force components achieve maximum magnitudes at $ka\approx 2$ and that these peaks are complicated by an oscillatory behaviour. These maxima correspond to a resonance in the forcing by the waves. When $ks=50$, F_{dxm} and F_{wxm} achieve maxima at about $ka=7{\cdot}0$ and monotonically decrease thereafter. The overall result is that as we increase the non-dimensional separation distance ks, the maxima of F_{wxm} and F_{dxm}, corresponding to x-compon-

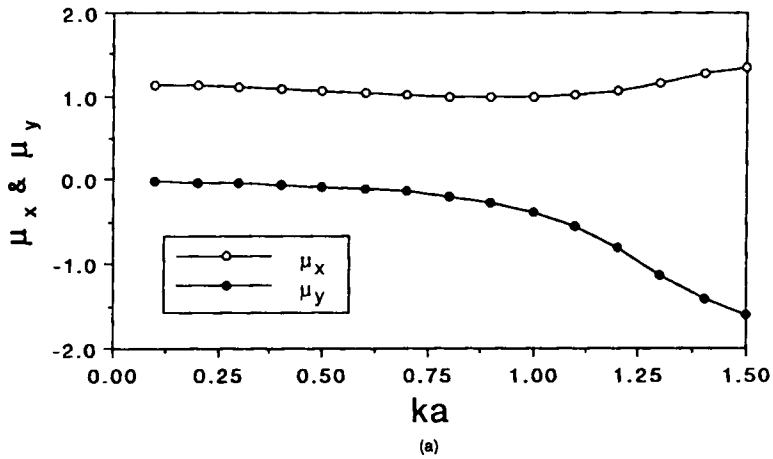

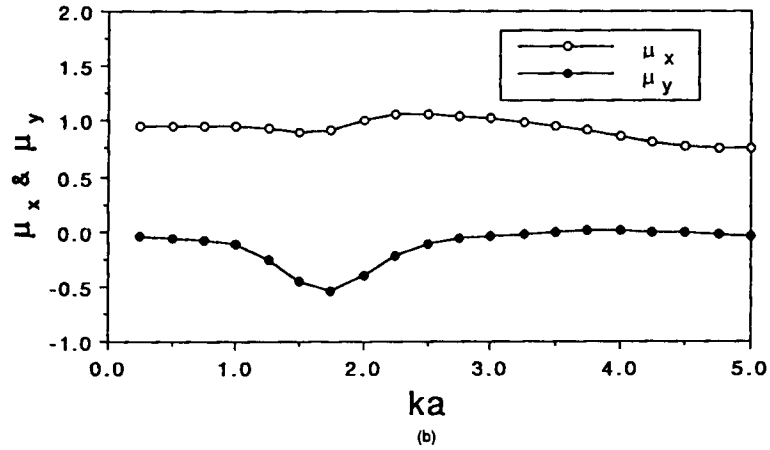

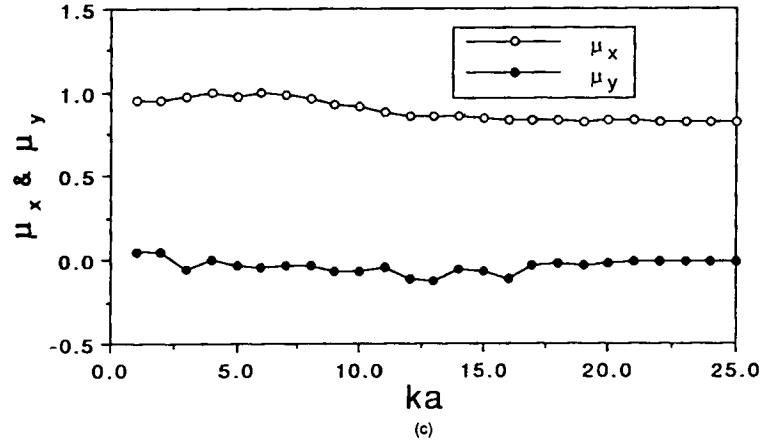

Figure 4. Amplification factors as a function of ka for $kh = 30$: (a) $ks = 3{\cdot}0$, (b) $ks = 10$, (c) $ks = 50$

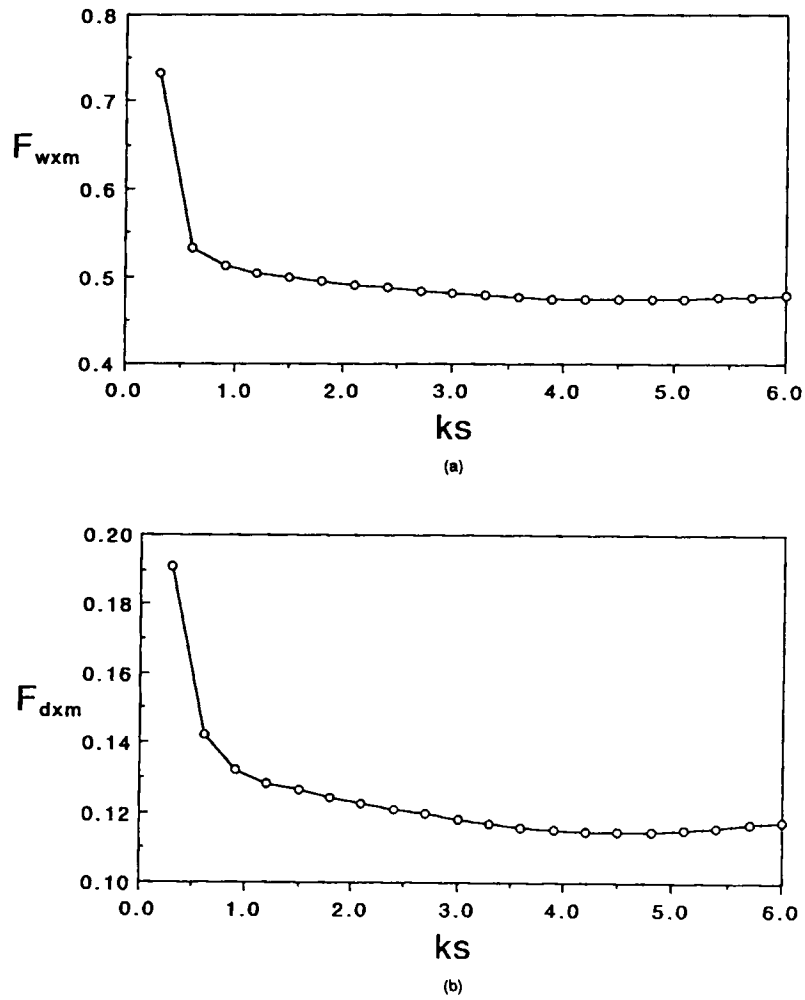

Figure 5. (a) Absolute maximum waterline force F_{wxm} and (b) absolute maximum dynamic force F_{dxm} as a function of ks for $ka=0{\cdot}15$, $kh=30$ and $A/a=2$

ent resonances in these forces, decrease. The maxima migrate to higher ka as ks increases, revealing a tendency (reminiscent of Figures 4(a)–4(c)) for maxima to occur at specific s/a-values.

The variation is F_{dym} and F_{wym} shown in Figures 8(a)–8(c) is more complicated. In the x-component case when $ks=3{\cdot}0$, Figure 8(a) shows that F_{wym} and F_{dym} have maxima at about ka, when the cylinders touch. Increasing the non-dimensional separation ks reduces these maxima and, as seen in Figure 8(b), demonstrates that they are resonance peaks at about $ka=1{\cdot}5$. Local maxima at $ka=5$, when the cylinders just touch, are also evident. Finally, when the non-dimensional separation distance is further increased, as in Figure 8(c) with $ks=50$, we obtain a family of resonance peaks for F_{wym} and F_{dym}. In each case the resonance magnitudes are reduced from the situation corresponding to smaller ks. The case when the cylinders just touch is no longer able to correspond to a resonance forcing, since the wavelength is now too small. We conclude that we need $ka<18$ for significant resonance forcing.

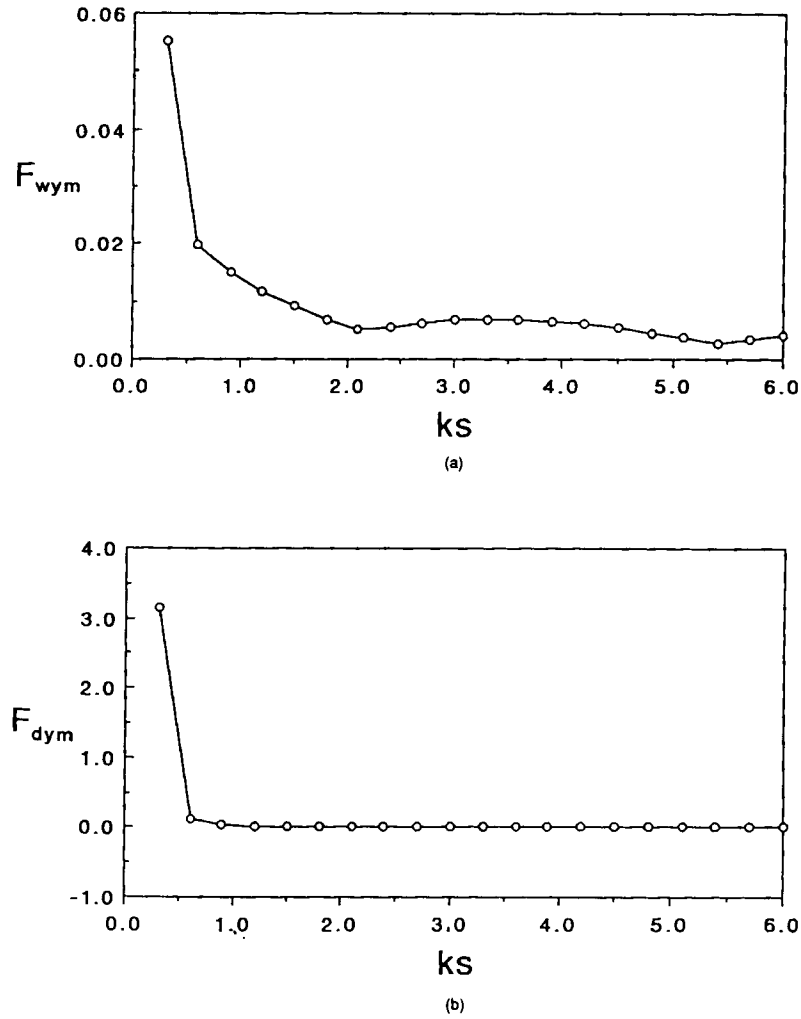

Figure 6. (a) Absolute maximum waterline force F_{wym} and (b) absolute maximum dynamic force F_{dym} as a function of ks for $ka=0{\cdot}15$, $kh=30$ and $A/a=2$

The variation in F_{dxm} and F_{dym} with kh is shown in Figures 9(a) and 9(b). While both become asymptotically quite large for small kh, F_{dxm} is clearly much larger than F_{dym} in magnitude. Interestingly, for $kh>1{\cdot}8$, F_{dxm} becomes negative.

In Figures 10(a)–10(d) we present the variation in the waterline force components F_{wx} and F_{wy} and the dynamic force components F_{dx} and F_{dy} in the x- and y-directions as a function of σt, non-dimensional time, for $ks=0{\cdot}3$ and $1{\cdot}5$. In each case the force component has about the same periodicity. We find that F_{dx} and F_{wx} experience peaks and troughs at about the same values of σt as do F_{dy} and F_{wy}. Qualitatively F_{dx} and F_{wx} have a similar variation with respect to σt, but in magnitude F_{wx} is about five times F_{dx}. Both F_{wx} and F_{dy} are about zero when $ks=1{\cdot}5$ with respect to variation in σt. Moreover, F_{dy} is about seven times F_{wy} in magnitude. While F_{wy} and F_{dy} are in phase, they are about one-sixth of a cycle out of phase with respect to F_{wx} and F_{dx}.

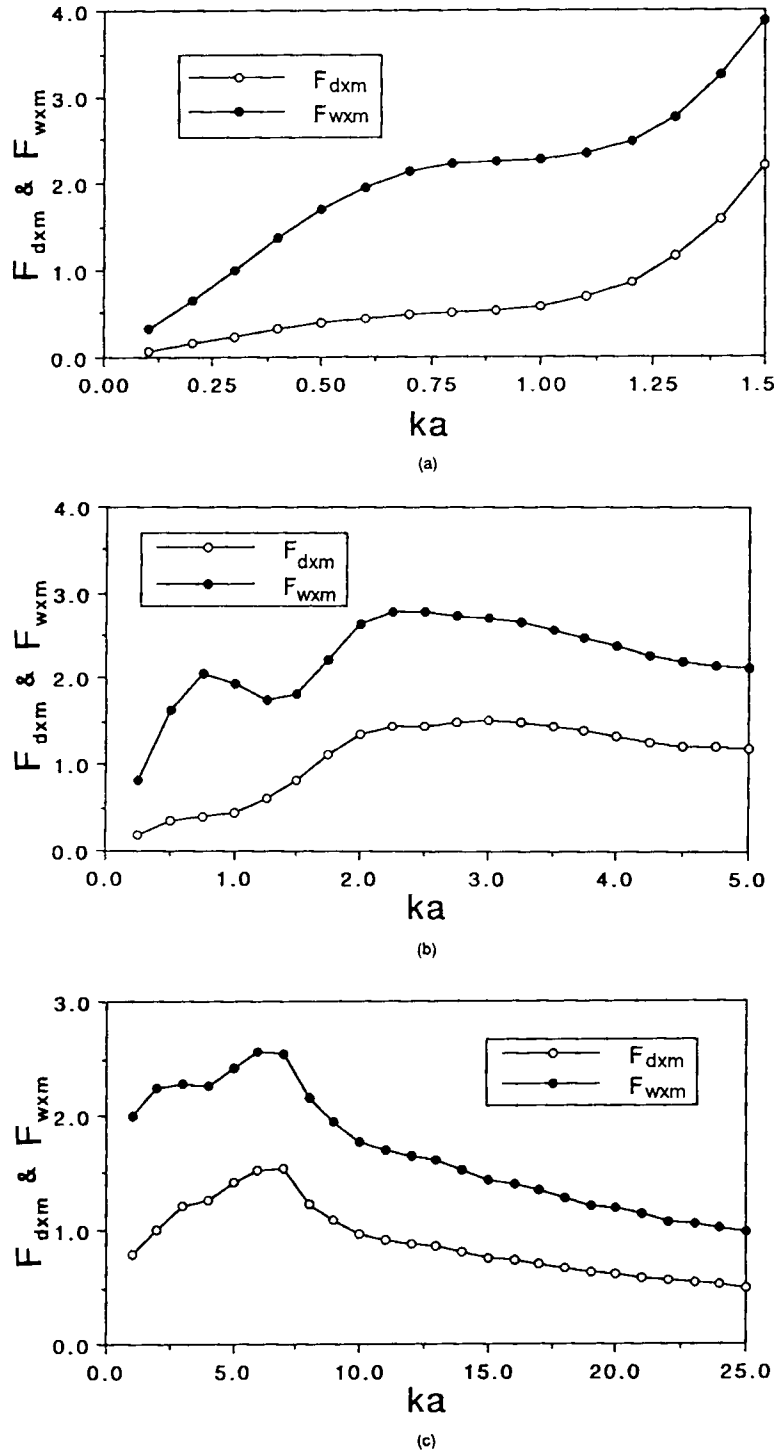

Figure 7. Absolute maximum waterline force F_{wxm} and absolute maximum dynamic force F_{dxm} as a function of ka for $kh=30$ and $A/a=2$: (a) $ks=3{\cdot}0$, (b) $ks=10$, (c) $ks=50$

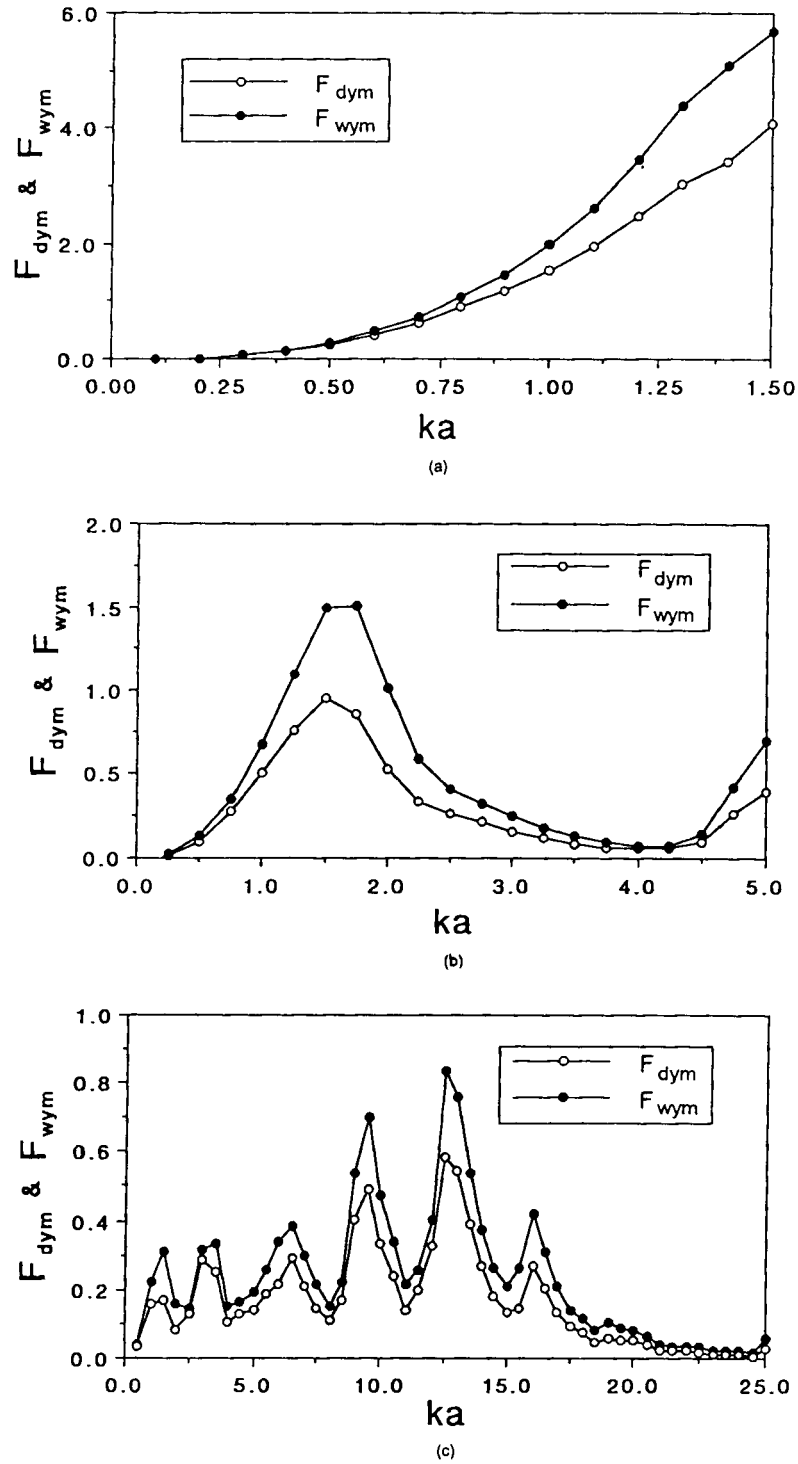

Figure 8. Absolute maximum waterline force F_{wym} and absolute maximum dynamic force F_{dym} as a function of ka for $kh = 30$ and $A/a = 2$: (a) $ks = 3{\cdot}0$, (b) $ks = 10$, (c) $ks = 50$

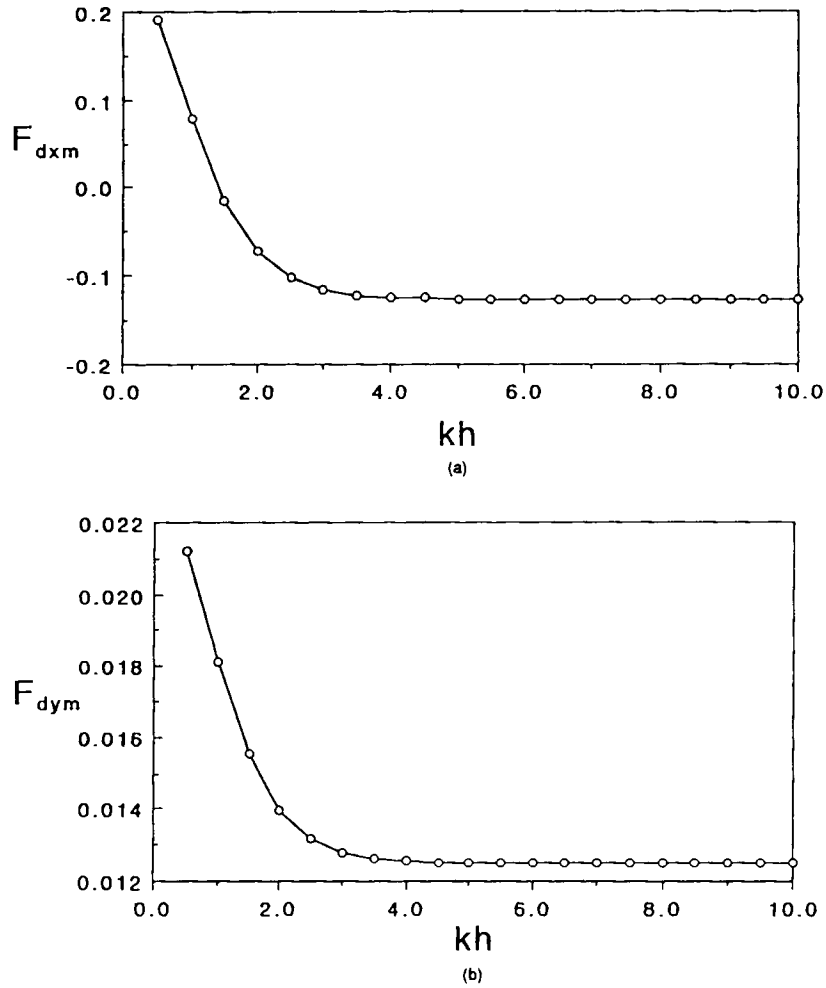

Figure 9. Absolute maximum dynamic forces (a) F_{dxm} and (b) F_{dym} as a function of kh for $ka=0{\cdot}15$, $ks=1{\cdot}5$ and $A/a=2$

CONCLUDING REMARKS

We have calculated the components of second-order drift forces for a pair of circular cylinders standing upright in finite depth water. Thus we have considered force components as functions of non-dimensional separation distance ks, non-dimensional radius ka and the ratio s/a, where s is the separation distance between the cylinders, a is the cylinder radius and k is the incident wave number. The resonances that are evident in our computations as a function of these variables ks, ka and s/a are the important results that we report.

The amplification factors μ_x and μ_y for the force components due to the presence of two cylinders compared to one cylinder, as a function of ks for different s/a-values, have oscillatory variations. While μ_y is normally smaller than μ_x over the domain of ks for which it was computed, μ_y is divergent as ks approaches zero. As functions of ka for given ks-values, μ_x and μ_y show distinctive resonances. When $ks=10$, these extrema become absolute over the domain of ka and

occur at about $ka = 1{\cdot}5$. When $ks = 50$, corresponding to a large separation distance, the extrema are still present and they exhibit smaller magnitudes than when ks is smaller in Figures 4(a) and 4(b). With increasing ks the resonances in μ_x and μ_y migrate to higher ka, suggesting a tendency for s/a to remain constant for resonance to occur. During resonance, μ_x is somewhat greater than unity whereas μ_y becomes negative, implying an attractive force relative to the one-cylinder situation.

For given ka-values the y-components of the dynamic and waterline forces, F_{dy} and F_{wy}, are almost zero with respect to variation in ks relative to the x-components F_{dx} and F_{wx}. All are divergent for small ks. As a function of ka for given ks-values, all components are similar in magnitude and, as seen in Figures 7(a)–7(c) and 8(a)–8(c), exhibit resonances. Analogously to μ_x, F_{dx} and F_{wx} experience a single extrenum which diminishes as ks assumes larger values. As ks increases, the resonances migrates to higher ka, implying a tendency for s/a to remain fixed.

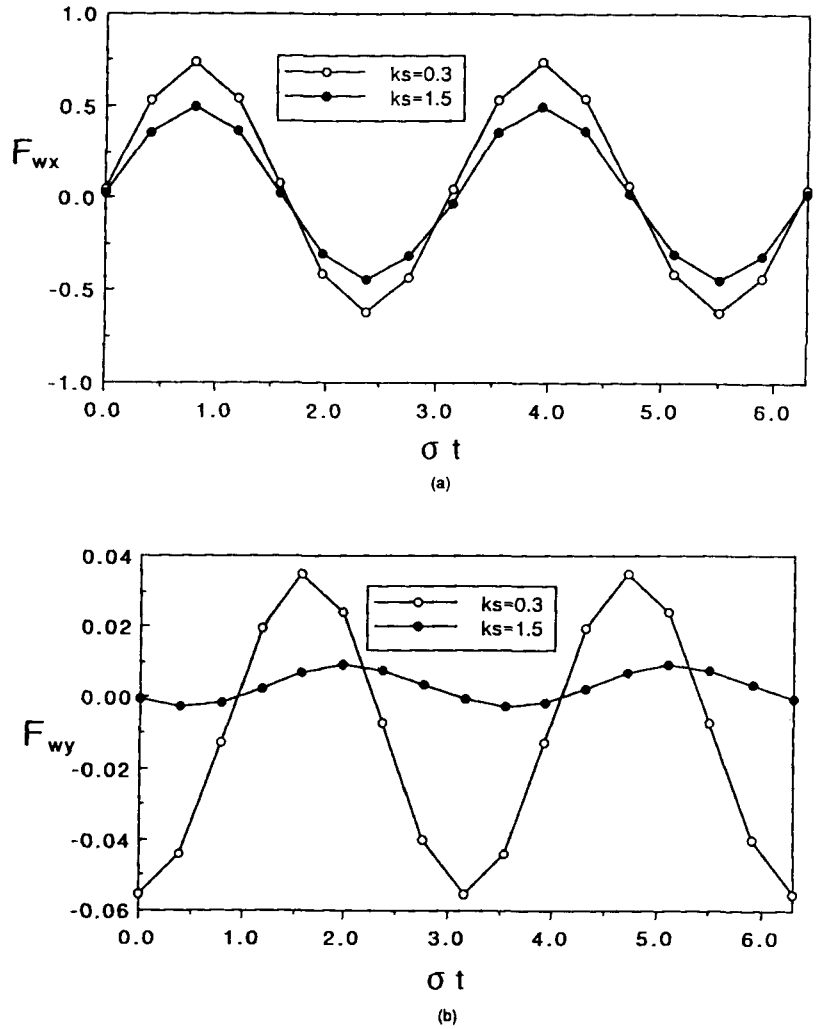

Figure 10. Total waterline forces (a) F_{wx} and (b) F_{wy} and total dynamic forces (c) F_{dx} and (d) F_{dy} as a function of σt for $ka = 0{\cdot}15$, $kh = 30$ and $A/a = 2$

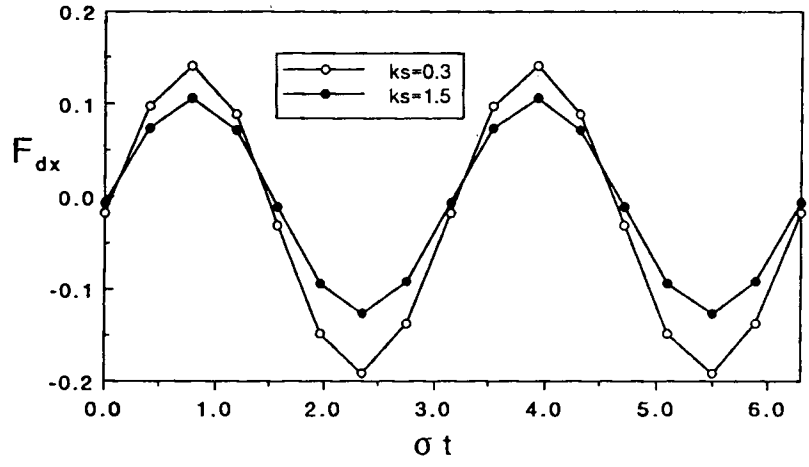

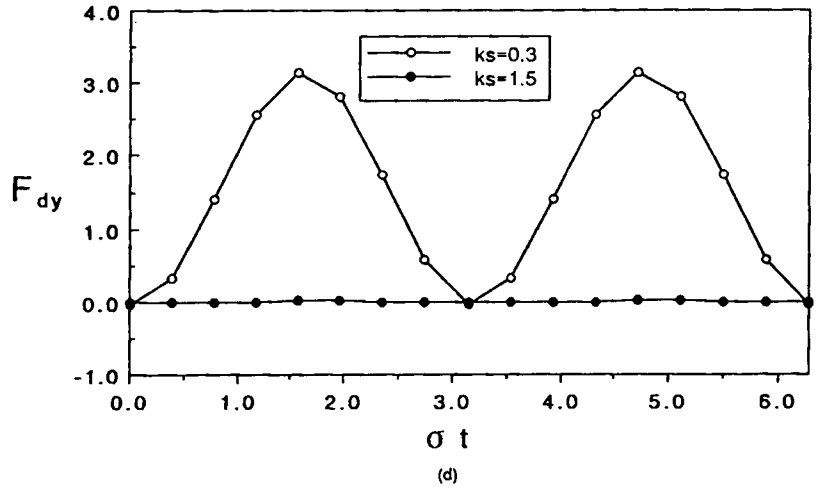

Figure 10. (Continued)

Multiple resonances are experienced by F_{dy} and F_{wy}, which also diminish in magnitude and move to higher ka-values as ks increases. With increasing ks, more 'subharmonics' of the initial resonance seen in Figures 8(a) and 8(b) become resonant, corresponding to the 'noisy' behaviour of μ_y in Figure 4(c).

Finally, both waterline and dynamic forces F_w and F_d are oscillatory in all their x- and y-components with respect to non-dimensional time σt. The x-component of F_w is several times the x-component of F_d, whereas the y-component of F_d is several times the y-component of F_w. In phase F_{wx} and F_{dx} agree and are offset relative to F_{wy} and F_{dy}, which also agree. Because of the unavailability of experimental data, the results presented in this paper cannot be compared for their correctness. However, a comparison with the preliminary results of Eatock-Taylor and Hung[17] shows fair agreement.

ACKNOWLEDGEMENTS

The authors are very grateful to the Natural Sciences and Engineering Research Council of Canada for financial support leading to this paper. The wave-modelling programme at BIO is funded by the Federal Panel on Energy Research and Development of Canada. We are also thankful to the referees for their constructive comments on the first version of this paper which help clarify some of the points in this paper.

APPENDIX: NOMENCLATURE

a	radius of cylinder
A	wave amplitude
C_M	Morison coefficient
F_l	linear force due to a single cylinder
F_w	second-order waterline force due to a single cylinder
F_d	second-order dynamic force due to a single cylinder
F	sum of forces F_d^{ss} and F_w^{ss} for a single cylinder
F_x, F_y	second-order steady state force components in the x- and y-directions for a pair of cylinders
$F_x^{(1)}, F_y^{(1)}$	first-order forces in the x- and y-directions for two cylinders
f	first-order force for a single cylinder
$F_{wx}^{(2)}, F_{wy}^{(2)}$	x- and y-components of second-order waterline forces (two cylinders)
$F_{dx}^{(2)}, F_{dy}^{(2)}$	x- and y-components of second-order dynamic forces (two cylinders)
F_w^{ss}, F_d^{ss}	steady state waterline and dynamic forces due to one cylinder
F_w^{os}, F_d^{os}	oscillatory waterline and dynamic forces due to one cylinder
F_{dw}^{ss}	total steady state (drift) forces due to waterline and dynamic forces (one cylinder)
F_{dw}^{os}	total oscillatory forces due to waterline and dynamic forces (one cylinder)
g	acceleration due to gravity
H	wave height
$H_n^{(2)}$	Hankel function of second kind of order n
h	water depth
J_n	Bessel function of first kind of order n
k	wave number
L	wavelength, $2\pi/k$
$\boldsymbol{n}$	unit outward normal
O_1	centre of cylinder 1
O_2	centre of cylinder 2
P	dynamic pressure
$\boldsymbol{q}$	velocity vector
r_1, θ_1	polar co-ordinates with respect to cylinder 1
r_2, θ_2	polar co-ordinates with respect to cylinder 2
s	distance between centres of two cylinders
ks	spacing parameter
ka	diffraction parameter
t	time
T	wave period
x	x-co-ordinate in horizontal plane
y	y-co-ordinate in horizontal plane

z	z-co-ordinate vertically upwards
∇	Laplacian operator
β	phase angle
η	wave elevation
λ_x	x-component first-order amplification factor
λ_y	y-component first-order amplification factor
μ_x	x-component second-order amplification factor
μ_y	y-component second-order amplification factor
ρ	density of water
Φ	velocity potential (real)
Φ_I	incident wave potential (real)
Φ_S	scattered wave potential (real)
ϕ_I	incident wave potential (complex)
ϕ_S	scattered wave potential (complex)
ϕ_{S1}	scattered potential due to cylinder 1 (complex)
ϕ_{S2}	scattered potential due to cylinder 2 (complex)
ϕ_i	velocity potential for a single cylinder similar to Φ
σ	incident wave frequency, $2\pi/T$

REFERENCES

1. K. Budal, 'Theory for absorption of wave power by a system of interacting bodies', *J. Ship Res.*, **21**, 248–253 (1977).
2. J. Falnes, 'Wave power absorption by an array of alternators oscillating with unconstrained amplitudes', *Appl. Ocean Res.*, **6**, 16–22 (1984).
3. M. Ohkusu, 'Wave actions on groups of vertical circular cylinders', in selected papers from *J. Soc. Naval Architect, Jpn.*, **11**, 37–50 (1973).
4. B. H. Spring and P. L. Monkmeyer, 'Interaction of plane wave with vertical cylinders', *Proc. 14th Int. Conf. on Coastal Engineering*, Copenhagen, 1974, pp. 1828–1847.
5. S. K. Chakrabarti, 'Wave forces on multiple vertical cylinders', *J. Waterways, Port, Coastal and Ocean Div., ASCE*, **104**, 147–154 (1978).
6. M. J. Simon, 'Multiple scattering in arrays of axisymmetric wave energy devices, Part 1: A matrix method using a plane wave approximation', *J. Fluid Mech.*, **18**, 273–285 (1982).
7. P. McIver and D. V. Evans, 'Approximation of wave forces on cylinder arrays', *Appl. Ocean Res.*, **6**, 101–107 (1984).
8. R. C. MacCamy and R. A. Fuchs, 'Wave force on piles: a diffraction theory', *Technical Memo* 69, Beach Erosion Board, Coastal Engineering Research Centre, U.S. Army, Washington, DC, 1954.
9. B. Molin, 'Second order diffraction loads on three dimensional bodies', *Appl. Ocean Res.*, **1**, 197–202 (1979).
10. R. Eatock-Taylor and S. M. Hung, 'Second order diffraction forces on a vertical cylinder in regular waves', *Appl. Ocean Res.*, **9**, 19–30 (1987).
11. M. Rahman, 'Wave diffraction by large offshore structures: an exact second order theory', *Appl. Ocean Res.*, **6**, 90–100 (1984).
12. M. Rahman, 'A design method of predicting second order wave diffraction caused by large offshore structures', *Ocean Eng.*, **14**, 1–8 (1987).
13. K. Masuda, W. Kato and H. Ishizuka, 'Second order diffraction loads on phase vertical cylinder with arbitrary cross sections', *Proc. 5th Int. OMAE Symp.*, Tokyo, 1986, pp. 345–352.
14. K. Masuda, W. Kato and C. Sakata, 'Nonlinear effects of surface waves on wave loads upon the plural vertical cylinder with arbitrary cross sections', *Proc. 6th Int. OMAE Symp.*, Houston, TX, 1987, pp. 72–81.
15. M. J. Lighthill, 'Waves and hydrodynamic loading', *Behaviour of Offshore Structures Conf., Boss* '79, London, 1979, pp. 1–40.
16. M. Abramowitz and I. Stegun, *Handbook of Mathematical Functions*, National Bureau of Standards, Dover, New York, 1964.
17. R. Eatock-Taylor and S. M. Hung, 'Wave drift enhancement effects in multicolumn structures', *Appl. Ocean Res.*, **7**, 128–139 (1985).